ELSEVIER

Chemical Engineering Journal 85 (2002) 7–15

Chemical Engineering Journal

www.elsevier.com/locate/cej

# Verification of the Maxwell–Stefan theory for tracer diffusion in zeolites

R. Krishna*, D. Paschek

*Department of Chemical Engineering, University of Amsterdam, Nieuwe Achtergracht 166, 1018 WV Amsterdam, The Netherlands*

Received 25 October 2000; received in revised form 17 January 2001; accepted 22 January 2001

**Abstract**

Using the Maxwell–Stefan theory for diffusion we derive a simple formula to relate the tracer (i.e. self) diffusivity $D^*$ and Maxwell–Stefan (MS), or jump, diffusivity $Đ$. The presence of the interchange coefficient $Đ_{ij}$ in the MS formulation causes the self diffusivity to be lower than the jump diffusivity. Assuming the interchange coefficient to be given by $Đ/F$ we derive:

$$D^* = \frac{Đ}{1 + F\theta}$$

where $F$ is a factor to take account of topology effects within the zeolite matrix.

The validity of the MS formulation is established by performing kinetic Monte Carlo simulations for diffusion of methane, perfluoromethane, 2-methylhexane and *iso*-butane in silicalite. Furthermore, it is shown that the exchange coefficient $Đ_{ij}$ is a quantification of correlation effects during the hopping of molecules. For *iso*-butane, the isotherm inflection leads to a sharp inflection in the diffusion behaviour. The influence of molecular repulsive forces on the loading dependence of the jump and self-diffusivities is also discussed with the aid of published Molecular Dynamics simulations for methane. 

*Keywords:* Maxwell–Stefan theory; Zeolites; Tracer diffusion; MD simulation

## 1. Introduction

The proper description of diffusive transport within zeolitic materials is of considerable importance in practice because of the many applications in catalytic reaction and separation processes [1–3]. Consider diffusion of a single component (1) within the matrix of a zeolite structure; the molecular flux, expressed in molecules per square meter per second, is given by

$$\boldsymbol{N}_1 = -\rho D \nabla \Theta_1 \tag{1}$$

where $\rho$ is the density of zeolite matrix, expressed in unit cells per cubic meter, $\Theta_1$ the molecular loading, expressed in molecules per unit cell. Eq. (1) defines the transport or Fick diffusivity $D$.

A more fundamental way of describing the diffusion process is to use chemical potential gradients as driving forces:

$$\boldsymbol{N}_1 = -\rho Đ \left( \frac{\Theta_1}{RT} \nabla_{T,p} \mu_1 \right) \tag{2}$$

where $Đ$ is variously referred to as the corrected, jump or Maxwell–Stefan (MS) diffusivity [1–4], $R$ the gas constant and $T$ the absolute temperature.

The Fick and MS diffusivities are inter-related by

$$D = Đ\Gamma \tag{3}$$

where $\Gamma$ is the thermodynamic correction factor [3,4]

$$\Gamma \equiv \Theta_1 \frac{\partial \ln P}{\partial \Theta_1} = \theta_1 \frac{\partial \ln P}{\partial \theta_1} \tag{4}$$

The adsorption isotherm relates the molecular loading $\Theta_1$ to the partial pressure of component 1 in the bulk gas phase surrounding the zeolite crystals, $P$. The Langmuir isotherm gives, for example:

$$\Theta_1 = \frac{\Theta_{1,\mathrm{sat}} bP}{1 + bP}, \qquad \theta_1 \equiv \frac{\Theta_1}{\Theta_{1,\mathrm{sat}}} = \frac{bP}{1 + bP} \tag{5}$$

where $b$ is the Langmuir constant, $\Theta_{1,\mathrm{sat}}$ the saturation loading and $\theta_1$ the fractional occupancy. For the Langmuir isotherm (5), the thermodynamic correction factor is given by

$$\Gamma = \frac{1}{1 - \Theta_1/\Theta_{\mathrm{sat}}} = \frac{1}{1 - \theta_1} \tag{6}$$

* Corresponding author. Tel.: +31-20-525-7007; fax: +31-20-525-5604.
*E-mail address:* krishna@its.chem.uva.nl (R. Krishna).

1385-8947/02/$ – see front matter 
PII: S1385-8947(01)00136-X

**Nomenclature**

| | |
|---|---|
| $D$ | Fick, or transport, diffusivity of component 1 in zeolite ($m^2\,s^{-1}$) |
| $Đ$ | Maxwell–Stefan, jump, or corrected, diffusivity of species $i$ in zeolite ($m^2/s$) |
| $Đ_{ij}$ | Maxwell–Stefan diffusivity describing interchange between $i$ and $j$ ($m^2/s$) |
| $D^*$ | tracer or self-diffusivity ($m^2/s$) |
| $F$ | factor introduced in Eq. (17), dimensionless |
| $k_i$ | transition probability ($s^{-1}$) |
| $n$ | number of diffusing species, dimensionless |
| $N$ | number of sorbed particles in KMC simulation, dimensionless |
| $\boldsymbol{N}_i$ | molar or molecular flux of species $i$, molecules $m^{-2}\,s^{-1}$ |
| $p_i$ | jump probability for $i$th process, dimensionless |
| $P$ | system pressure (Pa) |
| $\boldsymbol{r}$ | particle displacement vector (m) |
| $R$ | gas constant ($8.314\,J\,mol^{-1}\,K^{-1}$) |
| $T$ | absolute temperature (K) |
| $x_{i,A}$ | fraction of total loading of species $i$ in site A, dimensionless |
| $z$ | number of nearest neighbour sites, dimensionless |

*Greek letters*

| | |
|---|---|
| $\Gamma$ | thermodynamic correction factor, dimensionless |
| $\Theta_i$ | molecular loading, molecules per unit cell or per cage |
| $\Theta_{i,sat}$ | saturation loading, molecules per unit cell or per cage |
| $\Theta_{i,sat,A}$ | maximum loading of site A, molecules per unit cell |
| $\Theta_{i,sat,B}$ | maximum loading of site B, molecules per unit cell |
| $\lambda$ | lateral displacement (m) |
| $\mu_i$ | molar chemical potential ($J\,mol^{-1}$) |
| $\nu$ | jump frequency ($s^{-1}$) |
| $\theta_i$ | fractional surface occupancy of component $i$ |
| $\rho$ | density of zeolite, number of unit cells per $m^3$ |

*Subscripts*

| | |
|---|---|
| A | referring to site A |
| B | referring to site B |
| 1 | referring to untagged component 1 |
| 1* | referring to tagged component |
| int | intersections |
| sat | referring to saturation conditions |
| str | straight channel |
| zz | zig-zag channel |

In some cases, the sorption characteristics within the zeolite matrix is described by a two-site Langmuir (2SL) isotherm [4]:

$$\Theta_1 = \Theta_{1,A} + \Theta_{1,B} = \frac{\Theta_{1,sat,A} b_A P}{1 + b_A P} + \frac{\Theta_{1,sat,B} b_B P}{1 + b_B P} \tag{7}$$

where the subscripts 'A' and 'B' refer to two distinct types of sorption sites, each with its own saturation loading and Langmuir constant.

The thermodynamic factor $\Gamma$ for the 2SL isotherm is

$$\begin{aligned}\Gamma &= \frac{1}{(\Theta_{1,A}/\Theta_1)(1-(\Theta_{1,A}/\Theta_{1,sat,A})) + (\Theta_{1,B}/\Theta_1)(1-(\Theta_{1,B}/\Theta_{1,sat,B}))} \\ &= \frac{1}{x_{1,A}(1-\theta_{1,A}) + x_{1,B}(1-\theta_{1,B})}\end{aligned} \tag{8}$$

where $\theta_{1,A}$ and $\theta_{1,B}$ represent the fractional occupancies in the sites A and B, each normalised with respect to its own saturation capacity, and $x_{1,A}$ and $x_{1,B}$ represent the fractions of the total loading.

The Fick diffusivity $D$ is measured under *non-equilibrium* conditions in which finite gradients of the loading exist. They are determined by macroscopic methods like gravimetry, volummetry, chromatography or frequency response techniques [1,5]. In other experimental procedures, the *self*-diffusivities are measured under *equilibrium* conditions by microscopic techniques, viz. quasielastic neutron scattering and pulsed field gradient NMR. For self-diffusion, the flux of the marked, or tagged, species (1*) is measured under the influence of the gradient in the loading of marked molecules $\nabla\Theta_{1^*}$ keeping the total molecular loading (tagged and untagged species) constant ($\nabla\Theta_{1^*} + \nabla\Theta_1 = 0$):

$$\boldsymbol{N}_{1^*} = -\rho D^* \nabla\Theta_{1^*} \tag{9}$$

In the limit of zero loading the self, jump and transport diffusivities are all identical:

$$Đ = D^* = D, \qquad \Theta_1 \to 0 \tag{10}$$

In the published literature, there appears to be no general inter-relation between these three quantities under conditions of finite molecular loadings. In a recent experimental study, Jobic et al. [5] have found that $D > Đ > D^*$ for diffusion of $H_2$ in NaX zeolite. However, these authors did not provide any theoretical formulae for the inter-relationships. The objective of our paper is to try to develop a simple mathematical formula relating the three diffusivities using the Maxwell–Stefan theory for diffusion in zeolites. Such an inter-relation is very useful in practice, because self-diffusivities are easier to measure than the transport diffusivities. Since the transport diffusivities are the ones which are required in process design an inter-relation would allow these to be estimated more simply from self-diffusivity measurements. To validate the developed relations we perform kinetic Monte Carlo simulations of methane, perfluoromethane, 2-methylhexane and *iso*-butane in silicalite.

We also make use of published molecular dynamics (MD) simulation results in the literature.

## 2. The Maxwell–Stefan theory for tracer diffusion in zeolites

The essential concepts behind a general constitutive relation for diffusion in multicomponent mixtures were already available more than a century ago following the pioneering works of Maxwell [6] and Stefan [7]. These ideas have been applied to describe diffusion of $n$ species within a zeolite matrix using the following set of equations (for complete background, see [3,4,8–11]).

$$-\rho\frac{\theta_i}{RT}\nabla\mu_i = \sum_{\substack{j=1\\ j\neq i}}^{n}\frac{\Theta_j\boldsymbol{N}_i - \Theta_i\boldsymbol{N}_j}{\Theta_{i,\mathrm{sat}}\Theta_{j,\mathrm{sat}}\mathcal{Đ}_{ij}} + \frac{\boldsymbol{N}_i}{\Theta_{i,\mathrm{sat}}\mathcal{Đ}_i}, \quad i = 1, 2, \ldots, n \tag{11}$$

In the Maxwell–Stefan formulation for zeolite diffusion, Eq. (11), we have to reckon in general with two types of Maxwell–Stefan diffusivities: $\mathcal{Đ}_{ij}$ and $\mathcal{Đ}_i$. The $\mathcal{Đ}_i$ are the diffusivites which reflect interactions between species $i$ and the zeolite matrix; these correspond to the jump-diffusivities introduced earlier. Mixture diffusion introduces an additional complication due to sorbate–sorbate interactions. This interaction is embodied in the coefficients $\mathcal{Đ}_{ij}$. We can consider this coefficient as representing the facility for counter-exchange, i.e. at a sorption site the sorbed species $j$ is replaced by the species $i$. The net effect of this counter-exchange is a slowing down of a faster moving species due to interactions with a species of lower mobility. Also, a species of lower mobility is accelerated by interactions with another species of higher mobility.

Let us apply the above set of Eq. (11) for self diffusion and consider a system consisting of untagged (1) and tagged ($1^*$) species; see pictorial representation in Fig. 1. For self-diffusion the conditions of experiment are such that the gradients for diffusion of the tagged and untagged species are equal in magnitude and opposite in sign:

$$\nabla\theta_1 + \nabla\theta_{1^*} = 0 \tag{12}$$

and consequently the fluxes of tagged and untagged species sum to zero:

$$\boldsymbol{N}_1 + \boldsymbol{N}_{1^*} = 0 \tag{13}$$

Applying the restrictions (12) and (13) to Eq. (11) we obtain, after imposing $\mathcal{Đ}_1 = \mathcal{Đ}_{1^*} = \mathcal{Đ}$ for the tagged and untagged species:

$$\begin{aligned}\boldsymbol{N}_1 &= -\rho\Theta_{1,\mathrm{sat}}D^*\nabla\theta_1 \\ &= -\rho\Theta_{1,\mathrm{sat}}\frac{1}{(1/\mathcal{Đ})+((\theta_1+\theta_{1^*})/\mathcal{Đ}_{1,1^*})}\nabla\theta_1\end{aligned} \tag{14}$$

which shows that the tracer diffusivity $D^*$ is

$$D^* = \frac{1}{((1/\mathcal{Đ}) + (\theta/\mathcal{Đ}_{1,1^*}))} \tag{15}$$

where $\theta$ is the total occupancy (tagged and untagged species).

Eq. (15) shows that the tracer, self, diffusivity $D^*$ reduces to the Maxwell–Stefan diffusivity only when the interchange coefficient is exceedingly high:

$$D^* \to \mathcal{Đ} \text{ when } \mathcal{Đ}_{1,1^*} \to \infty \tag{16}$$

In the more general case for finite values of the exchange parameter $\mathcal{Đ}_{1,1^*}$ we would expect $D^*$ to be smaller than $\mathcal{Đ}$. The exchange parameter $\mathcal{Đ}_{1,1^*}$ is an expression of the *correlation* between the jumps of the tagged and untagged species. We should in general anticipate that the interchange coefficient is related in some way to the mobility of the species 1; we therefore take

$$\mathcal{Đ}_{1,1^*} = \frac{\mathcal{Đ}}{F} \tag{17}$$

where $F$ is a factor which could depend on the topology of the zeolite matrix. If no further information is available, we

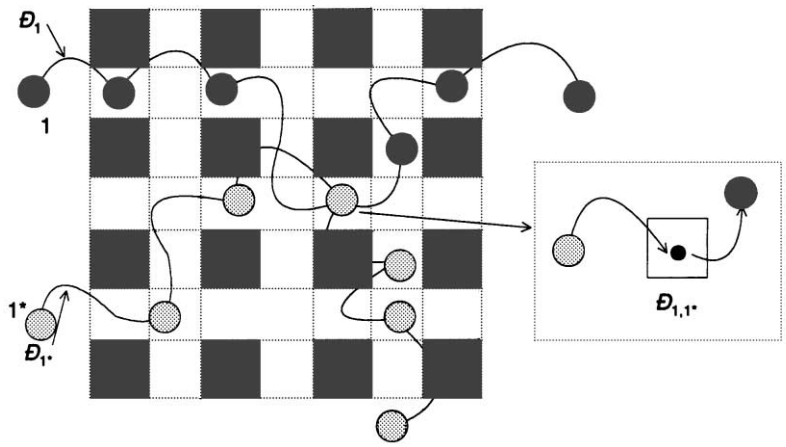


Fig. 1. Pictorial representation of self diffusion using the Maxwell–Stefan diffusion model.

could assume $F = 1$. We return later to the question of the proper estimation of this factor $F$. Combining Eqs. (15) and (17) we obtain the following working inter-relation between the tracer and jump diffusivity:

$$D^* = \frac{Đ}{1 + F\theta} \tag{18}$$

Both $Đ$ and $D^*$ are, in general, functions of the molecular loading within the zeolite. Consider the loading dependence of the jump diffusivity $Đ$. Mechanistically, $Đ$ may be related to the displacement of the adsorbed molecular species, $\lambda$, and the jump frequency, $\nu$:

$$Đ = \frac{1}{z}\lambda^2\nu \tag{19}$$

where $z$ represent the number of nearest neighbour sites. If we assume that a molecule can migrate from one site to another only when the receiving site is vacant, the chance that this will occur will be a function of the fraction of unoccupied sites. The loading dependence of the jump diffusivity is therefore.

$$Đ = Đ(0) \times [\text{Vacancy factor}] \tag{20}$$

where $Đ(0)$ represents the Maxwell–Stefan diffusivity in the limit of zero loading and

$$\text{Vacancy factor} = (1 - \theta_1); \quad \text{Langmuir isotherm} \tag{21a}$$

Additionally, molecular repulsive forces come into play when determining the jump frequency of molecules. Due to molecular repulsions the jump frequency increases because a molecule wishes to escape from the "unfavourable" environment. Clearly, the molecular repulsions will increase when the occupancy increases. Including molecular repulsions, we propose

$$Đ = Đ(0) \times [\text{Vacancy factor}] \times [\text{Repulsion factor}] \tag{22}$$

One simple model for repulsions would be to take:

$$\text{Repulsion factor} = \frac{1}{1 - \theta_1}, \quad \text{Langmuir isotherm} \tag{23a}$$

Combining Eqs. (22) with (21a) and (23a) we note that inclusion of repulsions leads to

$$Đ = Đ(0) \tag{24}$$

which shows that the jump diffusivity is independent of loading. This is indeed found to be true in several experimental studies [1,3,4].

The above relations for the vacancy factor and repulsion factor are valid for systems exhibiting Langmuir sorption characteristics. When the 2SL model holds, we expect the following relation for the vacancy factor

$$\text{Vacancy factor} = x_{1,\mathrm{A}}(1 - \theta_{1,\mathrm{A}}) + x_{1,\mathrm{B}}(1 - \theta_{1,\mathrm{B}}), \quad \text{2SL} \tag{21b}$$

and the repulsion factor:

$$\text{Repulsion factor} = \frac{1}{x_{1,\mathrm{A}}(1-\theta_{1,\mathrm{A}}) + x_{1,\mathrm{B}}(1-\theta_{1,\mathrm{B}})}, \quad \text{2SL} \tag{23b}$$

Even for the 2SL, the presence of repulsive forces will ensure that Eq. (24) holds and that the jump diffusivity will be independent of occupancy. When the repulsive factor shows a more complex dependence on the loading, we could expect the jump diffusivity to exhibit a more complex dependence on the occupancy [5].

We now seek verification of the validity of Eq. (18) by performing kinetic Monte Carlo simulations.

## 3. Kinetic Monte Carlo simulations with no repulsive interactions

We first performed kinetic Monte Carlo (KMC) simulations for diffusion of 2-methylhexane (2MH), methane ($CH_4$) and perfluormethane ($CF_4$) at 300 K in silicalite. Each component follows Langmuir isotherm behaviour and our KMC model does not take repulsive forces into consideration. We assume the lattice to be made up of equal sized sites which can be occupied by only one molecule at a time and there are no further molecule–molecule interactions. Particles can move from one site to a neighbouring site via hops. The probability per unit time to move from one site to another is determined by transition rates for the zig-zag (zz) and straight (str) channels; see Fig. 2 for a schematic sketch. For 2MH, the transition probabilities were determined based on the calculations of Smit et al. [12] and the procedure is described in detail in our earlier publications [13,14]. For $CH_4$ and $CF_4$, the transition probabilities were chosen to match the Molecular Dynamics simulation results of Pickett et al. [15] and Goodbody et al. [16]. Table 1 lists the input

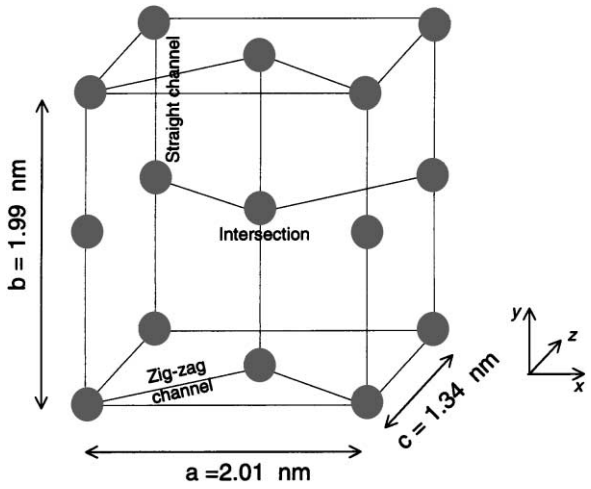


Fig. 2. Diffusion unit cell for silicalite connecting intersection sites (large black dots) via straight and zig-zag channels.

Table 1
Transition probabilities and zero-loading diffusivities for KMC simulations

| Species | 2MH | $CH_4$ | $CF_4$ | *Iso*-butane |
|---|---|---|---|---|
| Isotherm | Langmuir | Langmuir | Langmuir | Dual-site Langmuir |
| Saturation loading | 4 (at intersections) | 24 | 12 | 4 (at intersections), 8 (interior) |
| $k_{zz\rightarrow int}/[s^{-1}]$ | $5 \times 10^4$ | $1.8 \times 10^{12}$ | $2.05 \times 10^{10}$ | $4.0 \times 10^{10}$ |
| $k_{int\rightarrow zz}/[s^{-1}]$ | $5 \times 10^4$ | $1.8 \times 10^{12}$ | $2.05 \times 10^{10}$ | $6.68 \times 10^{6}$ |
| $k_{str\rightarrow int}/[s^{-1}]$ | $1.4 \times 10^4$ | $2.1 \times 10^{12}$ | $3.25 \times 10^{10}$ | $1.05 \times 10^{11}$ |
| $k_{int\rightarrow str}/[s^{-1}]$ | $1.4 \times 10^4$ | $2.1 \times 10^{12}$ | $3.25 \times 10^{10}$ | $1.75 \times 10^{7}$ |
| $Đ(0)/[m^2\ s^{-1}]$ | $6.86 \times 10^{-14}$ | $1.55 \times 10^{-8}$ | $3.33 \times 10^{-9}$ | $4.40 \times 10^{-12}$ |

data on the transition probabilities. For 2MH the maximum number of sorption sites per unit cell is 4 and the corresponding number for $CH_4$ and $CF_4$ are 24 and 12, respectively. These maximum loadings were taken on the basis of configurational-bias Monte Carlo simulation results of Vlugt et al. [17] and experimental data of Heuchel et al. [18].

We employ a standard KMC methodology to propagate the system (details in [13,14,19–21]). A hop is made every KMC step and the system clock is updated with variable time steps. For a given configuration of random walkers on the silicalite lattice a process list containing all possible $M$ moves to vacant intersection sites is created. Each possible move $i$ is associated with a transition probability $k_i$. Now, the mean elapsed time $t$ is the inverse of the total rate coefficient

$$\tau^{-1} = k_{\text{total}} = \sum_{i=1}^{M} k_i \tag{25}$$

which is then determined as the sum over all processes contained in the process list. The actual KMC time step $\Delta t$ for a given configuration is randomly chosen from a Poisson distribution

$$\Delta t = -\ln(u) k_{\text{total}}^{-1} \tag{26}$$

where $u \in [0,1]$ is a uniform random deviate. The timestep $\Delta t$ is independent from the chosen hopping process. To select the actual jump, we define process probabilities according to $p_i = \sum_{j=1}^{i} k_j / k_{\text{total}}$. The $i$th process is chosen, when $p_{i-1} < \nu < p_i$, where $\nu \in [0,1]$ is another uniform random deviate. After having performed a hop, the process list is updated. In order to sample ensemble averages correctly and to calculate dynamical properties more easily, the variable time scale is mapped on a periodic time scale for analysing purposes. In order to avoid surface effects we employ periodic boundary conditions. A choice of $5 \times 5 \times 5$ unit cells ensures freedom from finite size effects [13,14]. About $10^7$ simulation steps were performed for each simulation.

The self-diffusivity tensor is described by its components in the $x$-, $y$- and $z$-directions:

$$D_\alpha^* = \lim_{\Delta t\rightarrow\infty} D_\alpha^*(\Delta t) = \frac{1}{2} \lim_{\Delta t\rightarrow\infty} \frac{1}{\Delta t} \langle r_\alpha^2(\Delta t) \rangle \tag{27}$$

with $\langle \cdots \rangle$ denoting both ensemble and time averaging, $r_\alpha$ is the particle displacement vector and $\alpha$ is $x$, $y$ or $z$. Accordingly, the self-diffusion coefficient is expressed by

$$D^* = \tfrac{1}{3}(D_x^* + D_y^* + D_z^*) \tag{28}$$

Following the works of Reed and Ehrlich [19] and Uebing and coworkers [22,23] we also calculated the thermodynamic correction factor $\Gamma$ by relating it to the particle fluctuations in a finite probe volume:

$$\Gamma = \frac{\langle N \rangle}{\langle N^2 \rangle - \langle N \rangle^2} \tag{29}$$

at equilibrium conditions where $N$ is the number of adsorbed particles.

The MS-diffusivity was calculated from the KMC simulations using the following relation [17,20]:

$$Đ = \frac{1}{6} \lim_{\Delta t\rightarrow\infty} \frac{1}{\Delta t} \left\langle \left( \frac{1}{N} \sum_{i=1}^{N} (\mathbf{r}_i(t + \Delta t) - \mathbf{r}_i(t)) \right)^2 \right\rangle \tag{30}$$

which represents the mean square displacement of the center of gravity of the $N$ adsorbed particles.

Let us first consider the KMC simulations results for 2MH; see Fig. 3. We note that the KMC simulated $\Gamma$ follows the theoretical Langmuir behaviour $1/(1-\theta)$; see Fig. 3(a). The jump diffusivity $Đ$ shows a linear dependence on the fractional vacancy, in conformity with Eqs. (20) and (21a), and the transport $D$, is seen to be independent of occupancy; see Fig. 3(b). The self-diffusivity $D^*$ values from KMC simulations compare very well with the estimations from Eq. (18), taking $F = 1$.

The KMC simulation results for $CH_4$ are shown in Fig. 4. We note, again, that the KMC simulated $\Gamma$ follows the theoretical Langmuir behaviour $1/(1-\theta)$ and the jump diffusivity $Đ$ follows the loading dependence given by Eqs. (20) and (21a). The self-diffusivity $D^*$ determined from KMC simulations agree with the predictions of Eq. (18), taking $F = 2$. The reason for stronger correlation effect is to be found in the fact that for methane we have a total of 24 sorption sites compared to only 4 for 2MH. Put another way, the factor $F$ appears to be related to the topology of the system. If no a priori information is available we see that $F = 1$ also gives a reasonable estimate for the tracer $D^*$.

The KMC simulation results for the self-diffusivity values for $CF_4$ are shown in Fig. 5. The predictions of Eq. (18) works best taking $F = 1.5$. It is noteworthy that the best

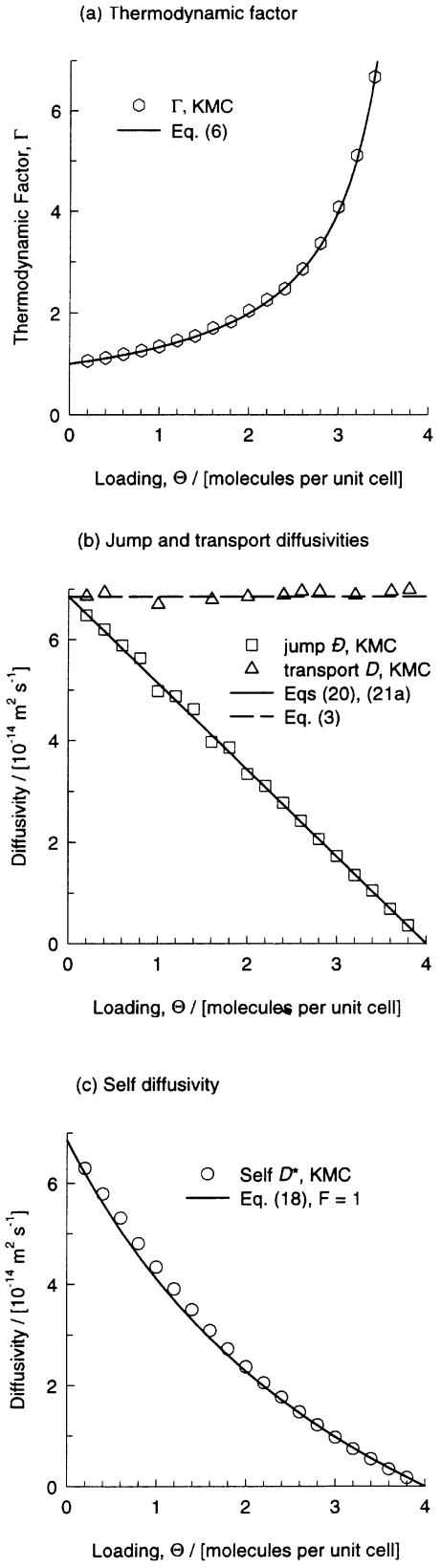


Fig. 3. Kinetic Monte Carlo simulations of thermodynamic factor, jump- and transport- and self-diffusivities of 2MH in silicalite at 300 K.

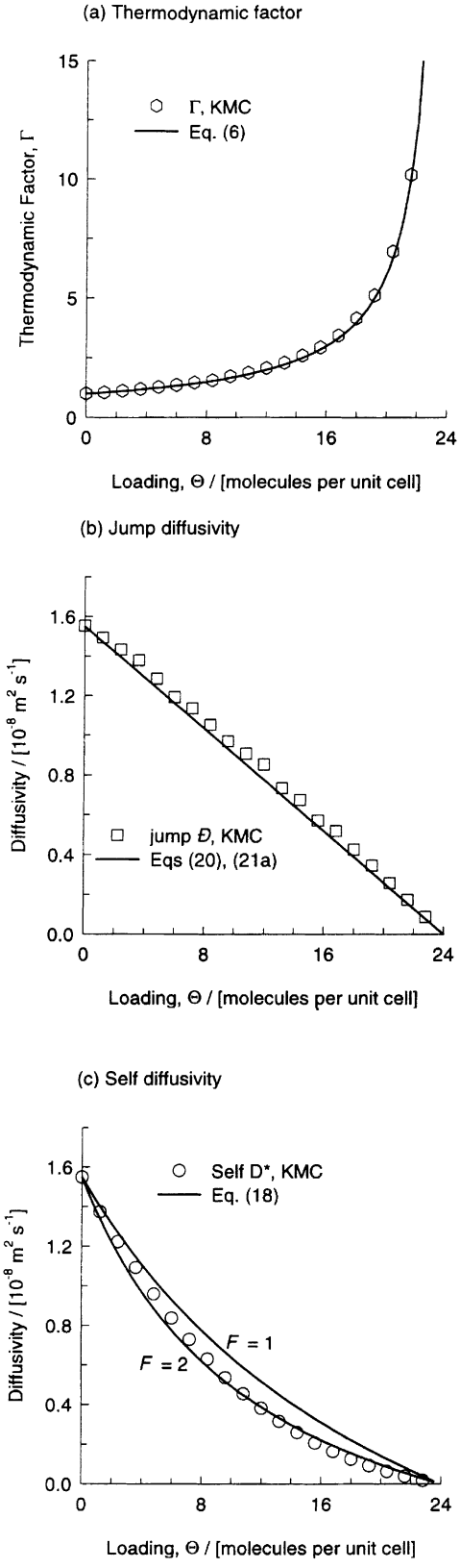


Fig. 4. Kinetic Monte Carlo simulations of thermodynamic factor, jump- and self-diffusivities of $CH_4$ in silicalite at 300 K.

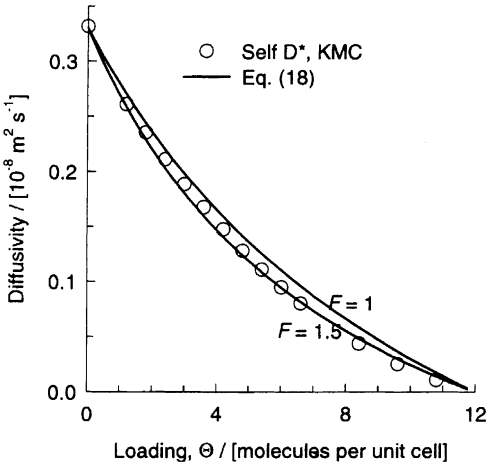


Fig. 5. Kinetic Monte Carlo simulations of self-diffusivity $CF_4$ in silicalite at 300 K.

fit values of $F$ seems to depend on the number of sorption sites. For we have a total of 12 sorption sites, intermediate between those for $CH_4$ and 2MH. The $F$ value for $CF_4$ is also intermediate between those for $CH_4$ and 2MH. Even $F = 1$ gives a good engineering model for the tracer $D^*$.

Let us now consider diffusion of *iso*-butane in silicalite at 300 K. In an earlier study using configurational-bias Monte Carlo (CBMC) simulations [17], we have shown that the sorption isotherm for *iso*-butane shows an inflection at a loading of four molecules per unit cell (see Fig. 6). This inflection is caused because *iso*-butane prefers to locate at the intersections. At a loading of four molecules per unit cell all the intersection sites are occupied and an extra "push" is required to force *iso*-butane to occupy the sites within the channel interiors (straight and zig-zag channels). As can be seen from Fig. 6, the dual-site Langmuir isotherm (7) is able

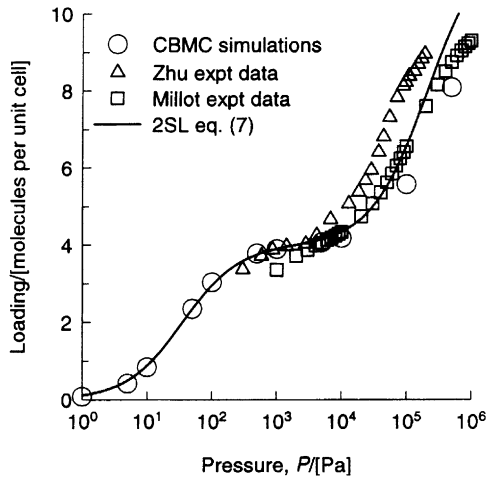


Fig. 6. Sorption isotherm for *iso*-butane at 300 K. Comparison of CBMC simulations [17] with experimental data [24,25]. The continuous line is the fitted dual-site Langmuir isotherm.

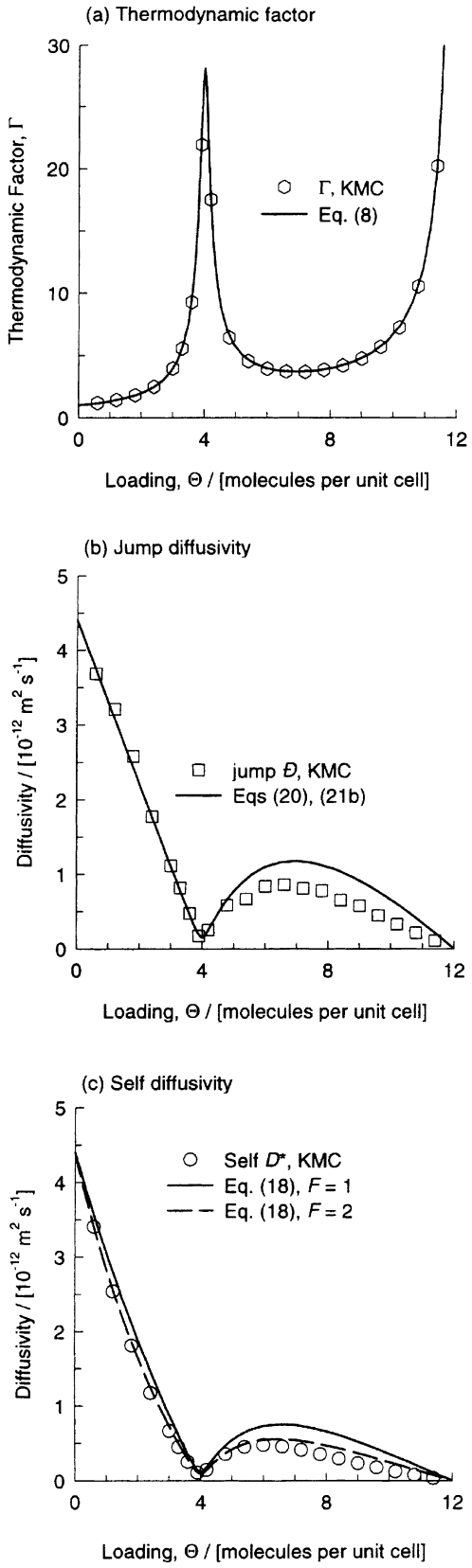


Fig. 7. Kinetic Monte Carlo simulations of thermodynamic factor, jump- and self-diffusivities of *iso*-butane in silicalite at 300 K.

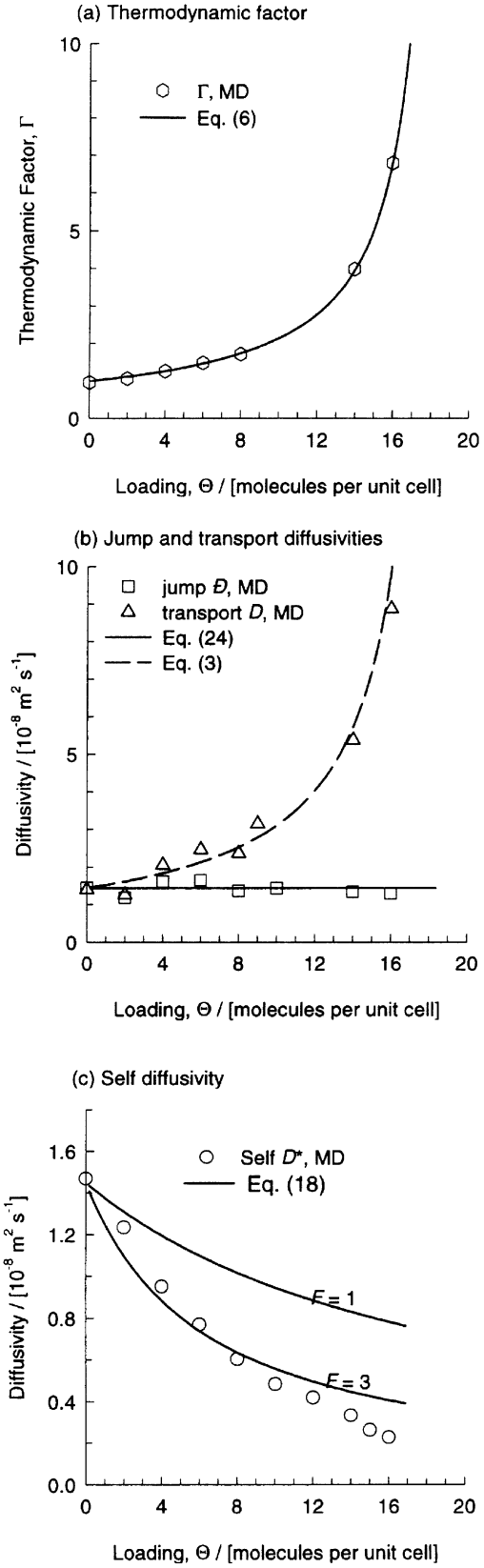


Fig. 8. Molecular dynamics simulations of thermodynamic factor, jump- and transport- and self-diffusivities of $CH_4$ in silicalite at 300 K; MD data from Maginn et al. [27].

to describe the isotherm very well; the CBMC simulations agree with the experimental data of Zhu et al. [24] and Millot et al. [25]. The dual-site parameters for *iso*-butane used in the fit shown in Fig. 6 are: $b_A = 0.028\,Pa^{-1}$, $b_B = 4.74 \times 10^{-6}\,Pa^{-1}$; $\Theta_{1,sat,A} = 4$, $\Theta_{1,sat,B} = 8$.

The experimental data of Millot et al. [26] for diffusion of *iso*-butane were used to choose the values of the transition probabilities in the straight and zig-zag channels. Furthermore, allowance was made for the preferential location at the intersections by assigning unequal transition probabilities to hops to an away from the intersections; see Table 1. For example, we have taken $k_{str\rightarrow int} = 1.05 \times 10^{11}\,s^{-1}$ and $k_{int\rightarrow str} = 1.75 \times 10^{7}\,s^{-1}$; the ratio $k_{int\rightarrow str}/k_{str\rightarrow int}$ is taken to be the ratio of the sorption strengths of the channel interiors and intersections, i.e. $b_B/b_A = 1.67 \times 10^{-4}$. The same ratio is also applied when assigning the transition probabilities to the hops to and away from the zig-zag channels.

Fig. 7 shows the KMC *iso*-butane simulation results for $\Gamma$, $Đ$ and $D^*$. We see from Fig. 7(a) that the KMC simulated $\Gamma$ follows precisely the theoretical trend predicted by Eq. (8) and shows a sharp maximum at $\Theta = 4$ molecules per unit cell, when all the intersection sites are completely occupied. The jump diffusivity $Đ$ follows closely the trend anticipated by Eqs. (20) and (21b) and shows a sharp dip at $\Theta = 4$; see Fig. 7(b). Eq. (18) with $F = 2$ gives a good representation of the KMC simulated $D^*$; see Fig. 7(c).

## 4. MD simulations for $CH_4$ including molecular repulsions

In the above KMC simulations for all four systems, no molecular repulsions were taken into account. We now consider the MD simulation results of Maginn et al. [27] for $\Gamma$, $Đ$, $D$ and $D^*$ which have been reproduced in Fig. 8. These MD simulations do take account of molecular repulsions. The simulated $\Gamma$ follows Langmuirian behaviour with a fitted value of $\Theta_{sat} = 18.76$ molecules per unit cell; see Fig. 8(a). It is interesting to note that the jump diffusivity is independent of loading. This is indicative of the fact that the repulsion forces are playing a role here and therefore Eqs. (22), (23a) and (24) are operational. The transport $D$, which is the product, $Đ\Gamma$ shows increases with $1/(1-\theta)$; see Fig. 8(b). The self-diffusivity values $D^*$ agree with the predictions of Eq. (18), provided we take $F = 3$. It appears that the correlation effects are additionally influenced by the presence of molecular repulsions.

## 5. Conclusions

Self-diffusivities in zeolites are strongly influenced by correlation effects, whereas the jump- and transport-diffusivities are both free from such effects. The Maxwell–Stefan diffusion theory has been used to derive a simple formula, Eq. (18), to relate the self-diffusivity to the

jump-diffusivity. KMC simulations for methane, perfluoromethane, 2-methylhexane and *iso*-butane in silicalite show the validity of the formula derived from the MS theory. The interchange coefficient $Đ_{1,1^*}$, in the MS formulation is an expression of correlation effects which also are affected by the system topology. Topology effects are taken into account by introducing a factor $F$ in Eq. (18). Our KMC simulation results show that $F$ increases from 1 to 2 when the number of sorption sites increases. For diffusion of *iso*-butane in silicalite, the isotherm inflection leads to an inflection in the diffusion behaviour; this is verified by KMC simulations.

When repulsive forces are taken into account, the jump diffusivity is independent of the fractional occupancy (cf. Eq. (24)) and the MD simulations for CH4, performed by Maginn et al. [27] confirm this trend. The MD simulated results also confirm the validity of Eq. (18) for tracer diffusion.

## Acknowledgements

The authors acknowledges a grant *Programmasubsidie* from the Netherlands Organisation for Scientific Research (NWO) for development of novel concepts in reactive separations technology.

## References

[1] J. Kärger, D.M. Ruthven, Diffusion in Zeolites and Other Microporous Solids, Wiley, New York, 1992.
[2] R. Krishna, B. Smit, T.J.H. Vlugt, Sorption-induced diffusion-selective separation of hydrocarbon isomers using silicalite, J. Phys. Chem. A 102 (1998) 7727–7730.
[3] R. Krishna, J.A. Wesselingh, The Maxwell–Stefan approach to mass transfer, Chem. Eng. Sci. 52 (1997) 861–911.
[4] R. Krishna, D. Paschek, Separation of hydrocarbon mixtures using zeolite membranes: a modelling approach combining molecular simulations with the Maxwell–Stefan theory, Separation Purification Technol. 21 (2000) 111–136.
[5] H. Jobic, J. Kärger, M. Bée, Simultaneous measurement of self- and transport-diffusivities in zeolites, Phys. Rev. Lett. 82 (2000) 4260–4263.
[6] J.C. Maxwell, On the dynamical theory of gases, Philos. Trans. R. Soc. 157 (1866) 49–88.
[7] J. Stefan, Über das Gleichgewich und die Bewegung, insbesondere die diffusion von Gasmengen, Sitzungsber. Akad. Wiss. Wien 63 (1871) 63–124.
[8] F. Kapteijn, J.A. Moulijn, R. Krishna, The generalized Maxwell–Stefan model for diffusion in zeolites: sorbate molecules with different saturation loadings, Chem. Eng. Sci. 55 (2000) 2923–2930.
[9] R. Krishna, T.J.H. Vlugt, B. Smit, Influence of isotherm inflection on diffusion in silicalite, Chem. Eng. Sci. 54 (1999) 1751–1757.
[10] R. Krishna, D. Paschek, Permeation of hexane isomers across ZSM-5 zeolite membranes, Ind. Eng. Chem. Res. 39 (2000) 2618–2622.
[11] R. Krishna, Diffusivity of binary mixtures in zeolites: MD simulations vs. Maxwell–Stefan theory, Chem. Phys. Lett. 326 (2000) 477–484.
[12] B. Smit, L.D.J.C. Loyens, G.L.M.M. Verbist, Simulation of adsorption and diffusion of hydrocarbons in zeolites, Faraday Discuss. 106 (1997) 93–104.
[13] D. Paschek, R. Krishna, Monte Carlo simulations of self- and transport-diffusivities of 2-methylhexane in silicalite, Phys. Chem. Chem. Phys. 2 (2000) 2389–2394.
[14] D. Paschek, R. Krishna, Diffusion of binary mixtures in zeolites: kinetic Monte Carlo vs. molecular dynamics simulations, Langmuir 17 (2001) 247–254.
[15] S.D. Pickett, A.K. Nowak, J.M. Thomas, B.K. Peterson, J.F.P. Swift, A.K. Cheetham, C.J.J. den Ouden, B. Smit, M.F.M. Post, Mobility of adsorbed species in zeolites—a molecular dynamics simulation of xenon in silicalite, J. Phys. Chem. 94 (1990) 1233–1236.
[16] S.J. Goodbody, K. Watanabe, D. MacGowan, J.R.P.B. Walton, N. Quirke, Molecular simulation of methane and butane in silicalite, J. Chem. Soc. Faraday Trans. 87 (1991) 1951–1958.
[17] T.J.H. Vlugt, R. Krishna, B. Smit, Molecular simulations of adsorption isotherms of linear and branched alkanes and their mixtures in silicalite, J. Phys. Chem. B 103 (1999) 1102–1118.
[18] M. Heuchel, R.Q. Snurr, E. Buss, Adsorption of $CH_4$—$CF_4$ mixtures in silicalite: simulation, experiment, and theory, Langmuir 13 (1997) 6795–6804.
[19] D.A. Reed, G. Ehrlich, Surface diffusivity and the time correlation of concentration fluctuations, Surf. Sci. 105 (1981) 603–628.
[20] K.A. Fichthorn, W.H. Weinberg, Theoretical foundations of dynamic Monte-Carlo simulations, J. Chem. Phys. 95 (1991) 1090–1096.
[21] C. Saravanan, S.M. Auerbach, Modeling the concentration dependence of diffusion in zeolites. 2. Kinetic Monte Carlo simulations of benzene in Na-Y, J. Chem. Phys. 107 (1997) 8132–8137.
[22] C. Uebing, V. Pereyra, G. Zgrablich, Diffusion of interacting lattice gases on heterogeous surfaces with simple topographies, Surf. Sci. 366 (1996) 185–192.
[23] E. Viljoen, C. Uebing, Effects of heterogeneity on the surface diffusion of interacting lattice gases: the bivariate trap model, Surf. Sci. 352 (1996) 1007–1011.
[24] W. Zhu, F. Kapteijn, J.A. Moulijn, Adsorption of light alkanes on silicalite-1: reconciliation of experimental data with molecular simulations, Phys. Chem. Chem. Phys. 2 (2000) 1989–1995.
[25] B. Millot, A. Methivier, H. Jobic, Modelling of adsorption equilibria of C4 to C7 alkanes in MFI type zeolites, Paper Presented at the 6th International Conference on Fundamentals of Adsorption, 24–28 May 1998, Elsevier, Paris, pp. 273–278.
[26] B. Millot, A. Methivier, H. Jobic, H. Moueddeb, M. Bee, Diffusion of isobutane in ZSM-5 zeolite: a comparison of quasi-electron neutron scattering and supported membrane results, J. Phys. Chem. B 103 (1999) 1096–1101.
[27] E.J. Maginn, A.T. Bell, D.N. Theodorou, Transport diffusivity of methane in silicalite from equilibrium and nonequilibrium simulations, J. Phys. Chem. 97 (1993) 4173–4181.